

## Interaction of low-energy electrons (1–30 eV) with condensed molecules: II. Vibrational-librational excitation and shape resonances in thin N<sub>2</sub> and CO films

L. Sanche and M. Michaud

*Groupe du Conseil de Recherche Médicale du Canada en Sciences des Radiations, Faculté de Médecine,  
Université de Sherbrooke, Sherbrooke, Québec, Canada J1H 5N4*

(Received 16 January 1984; revised manuscript received 22 June 1984)

Low-energy [(1–30)-eV] electron scattering in multilayer films of N<sub>2</sub> and CO, and in Ar matrices containing N<sub>2</sub>, was investigated using high-resolution electron-energy-loss spectroscopy (HREELS) and one-dimensional multiple scattering theory. The films were formed by condensing the gases on a polycrystalline platinum substrate held near a temperature of 20 K. Comparisons of experimental electron-energy-loss spectra in the range 0–2.4 eV with those generated theoretically indicated that the former are composed of peaks which result from single and multiple vibrational losses broadened by multiple phonon losses. The excitation function of the  $\nu=1-3$  vibrational levels of ground-state N<sub>2</sub> and CO were measured under different film conditions and angles of incidence of the primary beam. In CO the excitation functions exhibited broad peaks at 2.5 and 20 eV due to the formation of <sup>2</sup>Π and <sup>2</sup>Σ transient anions, respectively, similar to those previously found in N<sub>2</sub> films. From measurements of the intensity of the fundamental vibrational loss in N<sub>2</sub> as a function of film thickness, the total cross section for excitation of all possible vibrational levels of N<sub>2</sub> was found to be  $3.3 \times 10^{-16}$  cm<sup>2</sup> at resonance, and the sum of all phonon cross sections was found to be about  $5 \times 10^{-16}$  cm<sup>2</sup>.

### I. INTRODUCTION

This paper describes an experiment which detects vibrational excitation produced by the impact of low-energy [(1–30)-eV] electrons on thin diatomic molecular films (5–100 Å) deposited on a metal surface. The main objectives of this work are to provide a description of low-energy electron scattering in N<sub>2</sub> and CO multilayer films; in particular, to measure the energy dependence of the vibrational excitation processes and to study the role of electron resonances (i.e., transient negative ions) in populating the intermolecular and intramolecular vibrational states of these adsorbed molecules.

Electron resonances are formed by the interaction of a projectile electron with a target atom or molecule in which the electron is temporarily captured in the neighborhood of the target.<sup>1,2</sup> Such electron-target coupled states are abundant in electron scattering from gaseous atoms and molecules, where their formation is manifested by the presence of structures in the elastic or inelastic cross sections.<sup>1,3,4</sup> Depending on their lifetime, the observed structures exhibit experimental widths ranging from ~0.02 eV, due to the instrument's resolution, to several electron volts. Transient negative ions are usually divided into two major categories, depending on the state of the target to which the incident electron attaches.<sup>1</sup> *Shape* or *single-particle* resonances result from electron trapping by a potential connected with the ground state of an atom or molecule, whereas *core-excited* or "two-particle-one-hole" resonances are associated with an electronically excited state of the target. In molecular shape resonances the temporary binding of an extra electron in a usually unfilled orbital changes the interatomic forces, thus initiating nuclear motion. This effect causes an

enhancement in the excitation cross section for all possible vibrational levels of the ground state. Shape resonances can therefore be effectively detected by observing large increases in the energy dependence of the vibrational excitation cross sections. Such measurements have revealed the presence of shape resonances in a multitude of isolated electron-molecule systems,<sup>1,3</sup> but only recently have these states been observed in solids and in molecules adsorbed on metal surfaces.<sup>5–10</sup> We report here a detailed investigation of shape resonances occurring in N<sub>2</sub> and CO films under varying film conditions and scattering angles.

The apparatus and the conditions of operation are briefly described in the next section. The results are given in Sec. III, where the spectral features in energy-loss spectra are discussed in terms of the phenomenological multiple scattering theory formulated in our previous paper<sup>11</sup> (paper I). Shape resonances are identified as maxima in the vibrational excitation functions. Attempts are also made to estimate the magnitude of the total scattering cross sections. We give a discussion in Sec. III of the relaxation energies of condensed-phase transient anions and the effects of electron scattering on photoelectron spectra. Conclusions are given in Sec. IV

### II. EXPERIMENT

#### A. Apparatus

The energy-loss spectra and the energy dependence of vibrational energy losses are measured by high-resolution electron-energy-loss spectroscopy. The essential features of the experiment are the following. A monoenergetic electron beam emerging from an hemispherical monochromator is incident on a molecular film deposited on a

clean metal substrate; within a well-defined solid angle, a small portion of the electrons scattered out of the film are energy-analyzed by a hemispherical analyzer. The metal substrate is maintained near 20 K by an electrically isolated mechanical contact with the cold head of a closed-cycle refrigerated cryostat. This latter is mounted on a welded bellows equipped with precision adjusting screws. The arrangement allows *XYZ* positioning of the sample. The apparatus is housed in bakeable cryopumped ultrahigh-vacuum (UHV) system<sup>12</sup> capable of sustaining working pressures within the  $10^{-11}$ -Torr range.

The spectrometer is fundamentally similar to instruments employed in many laboratories, but does possess refinements which facilitate continuous measurement of various excitation functions. A scaled diagram of the experimental arrangement is shown in Fig. 1. The monochromator can be rotated between  $14^\circ$  and  $70^\circ$  from the normal of the sample and the analyzer is fixed at  $45^\circ$ . Energy dispersion is produced by applying a potential of about 1 V between two concentric hemispheres (10 and 11, and 30 and 31 in the figure). Imaging and energy control of the electron beam is achieved by means of electrostatic zoom lenses with cylindrical (14–16 and 26–28) and aperture electrodes (6–8 and 23–25). The dimensions and the focusing properties of both types of lenses were evaluated according to the analysis given by Harting and Read.<sup>13</sup> The source of electrons is a hairpin thoriated-tungsten filament (1) incorporated in a Soa-type immer-

sion lens<sup>14</sup> made of aperture 2 and anode 3. In order to correct electron trajectories perturbed by stray magnetic and electric fields, three pairs (4, 17, and 25) of mutually perpendicular deflection plates are inserted in the optics. Rings 13 and 33 can also modify and deflect trajectories inside the hemispheres.

Pulses from the electron multiplier (34) are amplified, shaped, and monitored with standard counting electronics coupled optically to a microcomputer. The latter, supervised by software packaging, controls the energy of the monochromator and the analyzer according to three different sweeping modes, and accumulates the corresponding counts by a variety of signal-averaging techniques. Three modes of operation are possible. Energy losses can be measured with constant initial or final energy by sweeping either the analyzer or the monochromator. Measurements of excitation functions are performed by sweeping both deflectors simultaneously while keeping a constant potential between them. By programming the second zoom stages (i.e., 18, 19, and 20, and 22, 23, and 24) of the lens system for constant magnification and focus while keeping the other stages (14, 15, and 16, and 26, 27, and 28) fixed, it is possible to achieve a nearly constant incident current density on the sample and transmission in the analyzer, over about an order of magnitude change in the target potential. For more extended energy sweeps, both stages are simultaneously swept or the first stage is readjusted between sweeps. Typical currents arriving on the target range from 0.5 to 5 nA for a corresponding overall resolution extending from 10 to 30 meV FWHM (full width at half maximum) of the elastically-scattered-electron distribution. The incident electron energy is calibrated within  $\pm 0.15$  eV with respect to the vacuum level by measuring the onset of electron transmission through the film and the onset of elastic reflection from the film surface.

Gases are introduced through a manifold which is isolated from the main vacuum chamber by an all-metal bakeable valve. This valve is connected to a tube having an opening located in front of the cryostat. The sample inlet manifold consists of two gas- or vapor-inlet tubes equipped with by-pass and precision leak valves connected to a small chamber whose volume (180 ml) is precisely known. This chamber can be evacuated by separate adsorption and ion pumping. The absolute pressure of the gases or vapors leaked into this chamber can be accurately measured by a capacitance manometer.

### B. Film preparation and characterization

The target metal substrate was cut from a polycrystalline platinum ribbon of 0.20 mm nominal thickness 2.0 by 1.0 cm. This material was supplied by the Ventron Corporation with a stated purity of 99.95%. The substrate was cleaned by resistive heating to temperatures near  $1500^\circ\text{C}$ . The temperature was monitored with an optical pyrometer. Heating in oxygen was also possible at a somewhat reduced temperature ( $900^\circ\text{C}$ ). These treatments gave energy-loss spectra which were absolutely free from vibrational energy losses due to contaminating atoms or molecules. In cases where the ribbon recrystallized in sufficiently large grains, it was possible to further check the

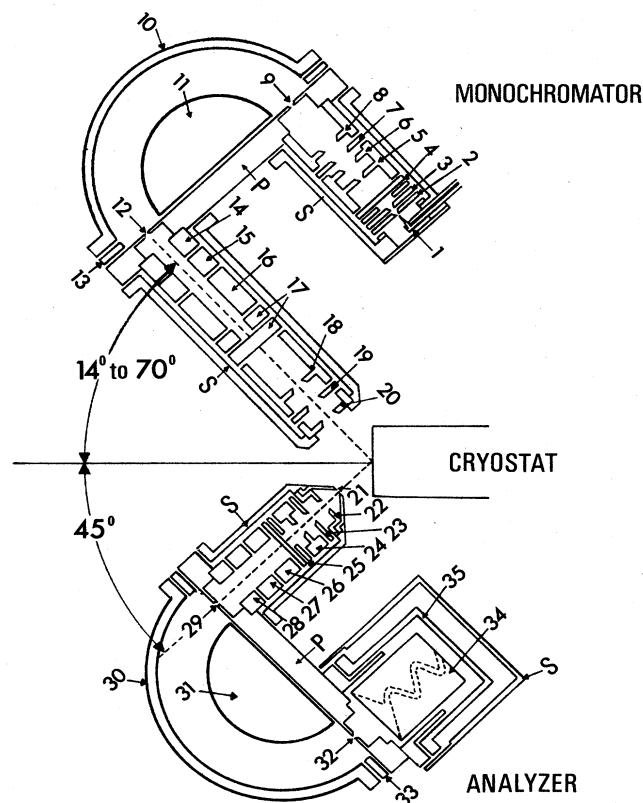


FIG. 1. Schematic diagram of hemispherical electron-energy-loss spectrometer.

purity of the surface and the resolution of the instrument by observing, in the specular beam, the fine interference structure which has been observed near the energy of the (01)-beam emergence threshold of the Pt(111) surface.<sup>15</sup>

The sample gases N<sub>2</sub>, CO, and Ar were purchased from Matheson of Canada, Ltd. with a stated purity of 99.9995%, 99.99%, and 99.99%, respectively. They were used without further purification. These gases, or a mixture of them, were leaked into a small chamber until a pressure of 0.05 Torr was reached. A calibrated amount of gas, given by the differential pressure drop and the known volume, was later expanded into vacuum. Assuming a sticking coefficient of unity it was possible to estimate the number of atoms or molecules which condensed on the substrate. From this method, described in detail by Chang and Berry,<sup>16</sup> and Madey,<sup>17</sup> we estimated the film thickness using bulk densities. A second approach consisted of measuring the change in work function of the substrate as a function of gas exposure. From this method<sup>18</sup> we determined the time and leak rate required to produce one monolayer. Using the calibrated values we estimated the film thickness, assuming no change in sticking coefficient with film growth. The percentage error is at least better than 40%. Experiments were conducted from submonolayer coverage to thicknesses up to 200 Å, in the case of matrices. The latter were produced by mixing small amounts of N<sub>2</sub> or CO with Ar in the calibrated chamber. The percentage volume in the matrices was calculated from the partial pressures of each gas and the ratio of the capillary conductance for different molecular masses.

The cryostat temperature (14 K) was measured by a hydrogen bulb welded around the cold tip. All experiments reported here were performed at this temperature. Owing to a temperature gradient between the substrate ribbon and the cold end of the cryostat, the temperature at the point of impact of the beam could not be measured precisely. However, from our ability to maintain solid films of N<sub>2</sub>, CO, and Ar at a constant thickness for hours in a vacuum of about  $5 \times 10^{-11}$  Torr, we concluded, by comparison with vapor-pressure data,<sup>19</sup> that the film temperature lay in the (14–20)-K range.

The geometrical arrangement of the film constituents could be varied according to the deposition rate and the condition of the metal substrate. Angular distribution measurements indicated that our films are polycrystalline, with many of the microcrystals oriented in the plane of the substrate. Crystals of N<sub>2</sub> and CO are known, from x-ray diffraction<sup>20,21</sup> and electron-diffraction measurements,<sup>22</sup> to exist in the  $\alpha$  state when grown around 20 K under reduced pressure. The structure is face-centered cubic with four molecules per unit cell. Both diagonal and off-diagonal disorder can be present in these crystals.<sup>23–25</sup> Owing to the crystalline nature of our films, energy-dependent variations in the intensity of energy-loss electrons were expected to be related not only to resonances but also to intermolecular interference phenomena. We differentiated between structure caused by long-range interference effects and electron resonances by varying the angle of incidence of the primary beam from 14° to 70°. At resonance, the additional electron is not characterized

by a well-defined momentum state of the solid, as is the case for coherently scattered electrons. The resonance energy is therefore independent of the incidence angle, whereas interference phenomena depend on the initial momentum of the electron.<sup>26</sup>

During the experiments periodic tests were made to ensure that the films did not charge due to electron trapping or space-charge effects in the dielectric. These phenomena could be detected by measuring energy shifts in the onset of the current transmitted through the films as a function of time and of primary beam intensity. Sanche, Bader, and Caron<sup>27</sup> have discussed this type of measurement in detail. For the spectra reported here we verified that trapped electrons or space charges did not alter the energy scales by more than 0.1 eV. Electron-beam damage, impurities, and chemisorption could have been detected by observing the appearance of vibrational modes other than those of the unperturbed target films. Neither time-dependent (due to electron-beam damage) nor time-independent extraneous modes were detected in the N<sub>2</sub> and CO films and Ar matrices.

### III. RESULTS AND DISCUSSION

#### A. Nitrogen

The energy-loss spectra for 3- and 20-eV electrons incident at 14° from the normal on a 50-Å-thick film are

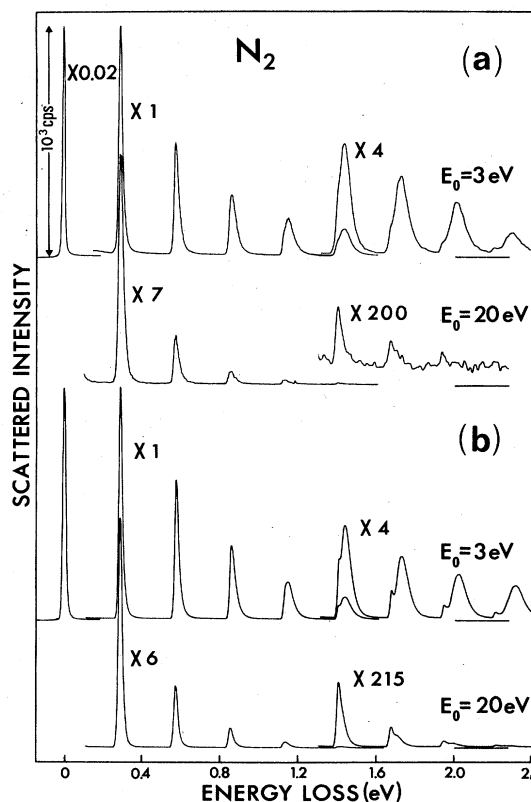


FIG. 2. (a) Energy-loss spectra for 3- and 20-eV electrons incident at 14° from the normal on a 50-Å-thick film. The gain for each curve is referenced to the  $\nu = 1$  loss at 290 meV in the top tracing. (b) Mathematical simulation of the spectra in (a) using the theory described in Ref. 11.

shown in Fig. 2(a). The vertical gain for each curve or portion of a curve is referenced to the  $\nu=1$  peak at 290 meV energy-loss in the top tracing. At an impact energy of 3 eV the energy-loss spectrum is composed of two overlapping series of vibrational levels. For  $\nu=1-4$ , the two progressions cannot be separated, but for higher vibrational losses ( $\nu=5-8$ ), sharp peaks become visible on the low-energy side of much broader and more intense energy-loss peaks. This type of spectrum has been previously reported in recent measurements by Schmeisser *et al.*<sup>10</sup> and by the present authors.<sup>7</sup> The latter found that the more intense progression exhibited a very small anharmonicity ( $x_e\omega_e=0.22$  meV), whereas the anharmonicity of the weaker series was typical of vibrational excitation of ground-state molecular nitrogen ( $x_e\omega_e=1.79$  meV) in the gas phase.<sup>28</sup> They interpreted the broad peaks as arising from excitation of vibrational levels of ground-state  $N_2$  accompanied by multiple intermolecular phonon transitions, but excluded the possibility of multiple vibrational losses. On the other hand, Schmeisser *et al.*<sup>10</sup> interpreted

the broad peaks as being due to multiple vibrational scatterings.

In this section we analyze the spectra in Fig. 2(a) in terms of the multiple scattering theory developed previously,<sup>11</sup> and attempt to reproduce mathematically the experimental data. Despite the apparent similarity between the spectra in Fig. 2(a) and those obtained with the same molecule in the gas phase,<sup>29</sup> two major differences exist: In the solid, the amplitudes of energy-loss peaks decrease much less, and their widths enlarge with increasing vibrational quantum number. These differences, which depend on the primary beam energy  $E_0$ , can be explained by multiple scattering effects.

For a semi-infinite film with large-angle electron scattering and a potential-barrier transmission coefficient  $T=1$  (i.e., no deflection at the surface of the film due to the inner potential), the total backscattered current-density distribution is given by formula (15) in Ref. 11, i.e.,

$$J(0,E) = \frac{1}{2} \int_{-\infty}^{\infty} I(0,E') \left[ \frac{Q_r(E-E')}{\alpha} + \frac{1}{2} \int_{-\infty}^{\infty} \frac{Q_r(E-E'')}{\alpha} \frac{Q_r(E''-E')}{\alpha} dE'' + \frac{5}{8} \int_{-\infty}^{\infty} \int_{-\infty}^{\infty} \frac{Q_r(E-E''')}{\alpha} \frac{Q_r(E'''-E'')}{\alpha} dE''' \frac{Q_r(E''-E')}{\alpha} dE'' + \dots \right] dE'. \quad (1)$$

$I(0,E')$  is the current density for electrons incident at energy  $E'$  on the film,  $E$  is the final energy, and  $E'',E''',\dots$  are the intermediate energies between collisions.  $Q_r(E-E')$  is the scattering probability per unit length and  $\alpha$  is the sum of the total scattering probability per unit length (i.e., the inverse mean free path). This series can be interpreted as a sum of partial current-density distributions, each term representing the contribution to  $J(0,E)$  originating successively from single, double, triple, . . . , collisions. The scattered intensity in single-collision gas-phase experiments would be described only by the first-order term in formula (1). The other terms represent multiple interactions, which, in a solid target, necessarily increase the scattered intensity. This qualitatively explains the higher intensity of energy-loss peaks in films compared to that in the gas phase.<sup>29</sup> Furthermore, the magnitude of this additional contribution depends on the product of terms composed of the ratio  $Q_r(E-E')/\alpha$ . When this ratio is large, the higher-order terms in (1) contribute significantly to the probed intensity. Since peaks resulting from multiple vibrational losses exhibit less anharmonicity, they occur at slightly different energies than the single-loss peaks of the corresponding overtone frequencies. Because of the many possible combinations of multiple and single vibrational and phonon losses, the overall effect leads to an appreciable increase of the width of peaks attributed to intramolecular vibrations. For example, at  $E_0=3$  eV in  $N_2$  films the vibrational peaks broaden appreciably as a function of vibrational quantum number. At these energies the ratio  $Q_r(E-E')/\alpha$  is large since only vibrational and phonon transitions are energetically

possible. However, when the incident energy is increased to 20 eV many electronic transitions become energetically possible and contribute to the increase of  $\alpha$ , whereas the vibrational excitation probability which contributes significantly to  $Q_r(E-E')$  is sensibly smaller than at  $E_0=3$  eV. We therefore observe a sharpening of the vibrational peaks which exhibit an anharmonicity characteristic of ground-state  $N_2$ .

In order to explain the results more quantitatively, we calculated  $J(0,E)$  according to the procedure described in Ref. 11 using energy losses taken from the optical spectra<sup>30,31</sup> of solid  $\alpha$ - $N_2$  and values of  $Q_r(E-E')$  and  $\alpha$  chosen to give the best fit in amplitude, width, and line shape. When the function  $Q_r(E-E')$  was taken as the energy-loss probability per unit length for losses  $E-E'$  corresponding only to vibrational excitation and  $\alpha$  as the sum of these probabilities in addition to an elastic scattering probability, it was impossible to generate the experimental shapes and widths of the top curve in Fig. 2. In other words, they could not simply be reproduced by self-folding the linewidth of the  $\nu=1$  loss and that of a combination of other vibrational losses, even though we convoluted each peak by a 10-meV FWHM Gaussian to reproduce the beam resolution. This result could be foreseen since it is difficult to imagine how, for example, the 19-meV FWHM  $\nu=1$  peak could give a width of 90 meV for  $\nu=8$  by self-folding. Nevertheless, the calculations indicated the the broad peaks involved multiple vibrational losses.

In subsequent calculations the quasielastic losses (i.e., librational plus translational phonons) of solid  $\alpha$ - $N_2$ ,<sup>30,31</sup>

which are dominated by 4- and 8-meV librational excitations, were considered in addition to intramolecular vibrational losses. Contributions from acoustic phonons, inhomogeneous broadening, and combination losses were neglected. The energies and relative amplitudes of seven phonon losses were taken from optical measurements to initiate our calculations. Good fits were obtained for vibrational amplitudes close to the gas-phase values<sup>32</sup> at 2.5 eV incident electron energy and a class of distributions of phonon amplitudes corresponding to a single 8-meV effective libron normalized to the sum of the phonon amplitudes. The computed result [i.e.,  $J(0, E)$ ] for such an effective distribution injected in  $Q_r(E - E')$  with vibrational amplitudes is shown in the upper curve of Fig. 2(b). The calculation was carried out taking into account 100 terms (i.e., up to 100 collisions per electron) in expression (1). The distribution was composed of one libron at 4 meV, one at 8 meV, and five between 10 and 14 meV, with relative amplitudes in the ratios 4:2:1, respectively. The total scattering probability of all phonons was taken to be equal to 1.5 of the sum of the vibrational scattering probabilities. The relative vibrational scattering probabilities were chosen close to the experimental values and the sum of the total fixed at 18% of  $\alpha$ . The total elastic probability was taken to be 54% of  $\alpha$ . As seen from comparisons in Fig. 2, the calculated curve closely resembles the experimental spectrum. Here, no attempt has been made to reproduce the intensity of the elastic peak, since an unknown contribution is due to the residual specular reflectivity of the polycrystalline film. Corrections on the sharp peaks, which appear better resolved in the calculated curve, could not be made by simply increasing the probability of librational losses while keeping the remaining characteristics the same. This discrepancy could only be resolved either by introducing in the calculation, through the formula (13) in Ref. 11, a smaller transmission coefficient for the potential barrier, or by splitting the probability of vibrational losses into vibrational-librational combinations. The fit of the peak widths is shown in Fig. 3, where the experimental and theoretical FWHM's of each energy-loss peak are plotted as a function of vibrational quantum number. Beyond  $v=5$  the sharp progression no longer enters into the measurement of the FWHM and, consequently, a break appears at  $v=5$  in Fig. 3. It is interesting to note that the ratio, 1.5, of the sum of all phonons to the sum of all vibrational scattering probabilities, which seemed essential to adequately reproduce the experimental data, is of the same order of magnitude as the ratio of about 0.75 found for the sum of the total rotational<sup>33</sup> to the sum of the total vibrational-rotational cross sections<sup>34</sup> found for  $N_2$  gas.<sup>35</sup> Although no precise allocation in the magnitude of each librational mode can be made from our analysis, we note that the best fits require peak amplitudes much different than those found in infrared<sup>36</sup> and Raman spectra<sup>31,37</sup> of  $\alpha$ - $N_2$ . In conclusion, the broad peaks in the simulated spectrum for incident energies  $E_0=3$  eV arise from multiple vibrational losses and the sharper series arise from single vibrational losses. Both series are broadened by multiple librational transitions, including, possibly, a small contribution from lower-energy phonon losses.

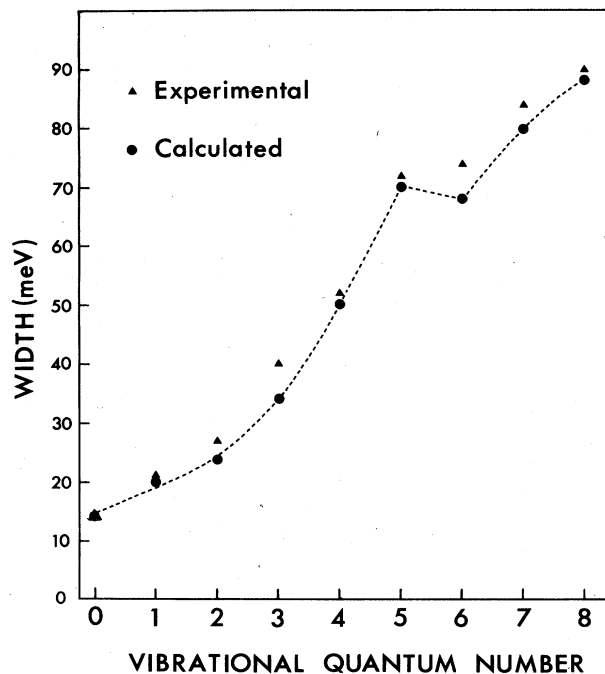


FIG. 3. Comparison between the experimental and calculated widths of vibrational losses  $v=1-8$  shown in Fig. 2.

Librational losses also displace the position of vibrational peaks toward higher energies. From our calculation we find that the  $v=1$  level is shifted by 2 meV toward higher energies. Applying this correction, the actual fundamental frequency in the solid is 288 meV, which corresponds to the gas-phase value.<sup>28</sup> At other impact energies a similar shift is observed, indicating that librational broadening may still play an important role even when resonance scattering decreases considerably. The calculated anharmonicity confirms the previous spectroscopic analysis<sup>7</sup> of the  $E_0=3$  eV spectra, and reveals that within the precision of the measurements (i.e.,  $\pm 1$  meV on peak position and  $\pm 0.15$  meV on anharmonicity) the vibrational well for  $N_2$  in the 50-Å-thick film is the same as that in the gas phase.

The energy-loss spectrum at  $E_0=20$  eV is composed of only a weak series corresponding to the sharp progression in the spectrum at  $E_0=3$  eV. As previously mentioned, at this primary energy we must take into account, in our calculation, additional higher-energy losses from electronic excitation which do not appear explicitly in the spectrum. Including the latter in  $\alpha$  reduces the ratio  $Q_r(E - E')/\alpha$  and enhances the amplitude of single over multiple vibrational losses. As an example, we show the bottom spectrum in Fig. 2, which has been obtained by modifying the  $E_0=3$  eV calculation by reducing the total scattering probability for  $v=1$  from 9% to 2% of  $\alpha$ , while keeping the relative vibrational amplitudes close to the experimental values and assuming that 25% of the collisions are electronic. The total librational and elastic

scattering probabilities were both fixed at 36% of  $\alpha$ . The line shape and the overall intensity of the theoretical curve closely resembles the experimental result for  $E_0=20$  eV. When contributions to electronic excitation are further increased to 50% or more of  $\alpha$ , very slight broadening and tailing of the vibrational peaks occurs. In other words, when other higher-energy excitation processes compete appreciably with librational and vibrational excitation, multiple losses are not apparent in energy-loss spectra.

Another interesting curve is generated when contributions to electronic excitation are set equal to zero while keeping the relative probability of the other parameters the same as those needed to produce the  $E_0=20$  eV curve. In this case the inelastic processes are dominated by librational losses and the resulting vibrational peaks appear much broader than those in any of the spectra in Fig. 2. Experimentally, this situation corresponds to electron scattering with primary energies in the (5–6)-eV range, where the collision probabilities for electronic losses are null and those for vibrational losses are small compared to the librational and elastic ones. *In this range, we do indeed observe a much larger broadening of all vibrational levels of ground-state  $N_2$ .*

Further evidence of the occurrence of multiple scattering is provided by observing the  $v=5-8$  vibrational levels of  $N_2$  in rare-gas matrices. The spectra in Fig. 4(a) were recorded at  $E_0=3$  eV for 50-Å-thick films of  $N_2$  and 50-Å-thick Ar matrices containing 10 and 5 vol %  $N_2$ . The vertical gains are referenced to the  $v=1$  peak at the top of Fig. 3, and the angle of incidence is  $14^\circ$  from the normal. The horizontal bars indicate the zero level for each curve. In the matrix the amplitude of the broad peaks relative to those of the sharp progression decreases rapidly with a lowering of  $N_2$  concentration, whereas the amplitude of the weak series is not noticeably altered. Attempts to calculate the energy-loss spectra in the matrix are shown in Fig. 4(b). The simulated curves for 10 and 5 vol %  $N_2$  were produced by simply increasing the probability of elastic collisions by a factor of 10 and 20, respectively, while keeping the other parameters from the pure-film calculation at  $E_0=3$  eV constant. We find that the trend in the relative amplitude of the different progressions is well represented, except for a factor of 2 in the intensity of the 5-vol % curve and a less pronounced broadening of the peaks. Our neglect of the phonon modes of the Ar matrix could possibly account for the major differences. As in the experiment, we find little decrease in the amplitude of the sharp progression relative to the broad series with decreasing  $N_2$  concentration. This result simply reflects the fact that an increase in the average number of elastic collisions increases the probability for the electron to be scattered out of the film between inelastic events, thus essentially reducing only the probability of higher-order inelastic processes. This type of behavior is discussed quantitatively in Ref. 11, where we derive a simple analytical expression for the backscattered current density related to single and double large-angle inelastic collisions in the multiple elastic scattering regime.

The variation in the *integrated* current distribution of each energy-loss peak exhibits approximately the same general trend as a function of thickness: a linear rise, at

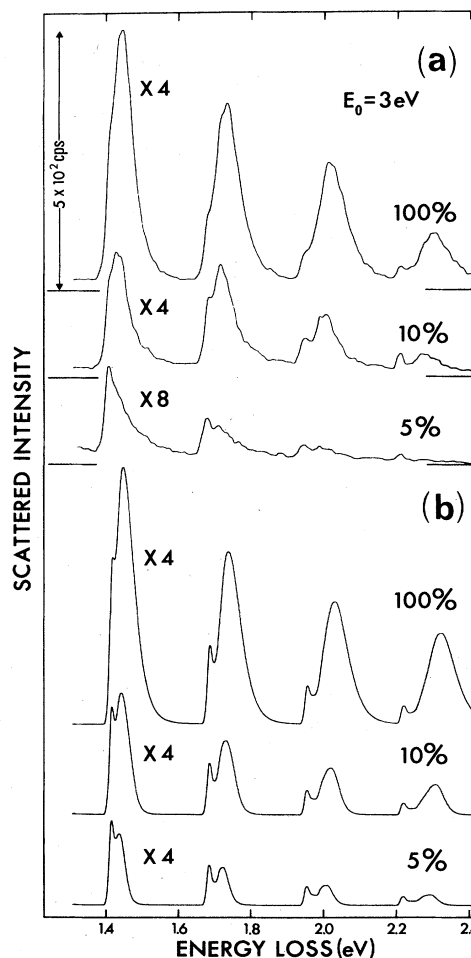


FIG. 4. (a) Energy-loss spectra for 3-eV electrons incident on a pure- $N_2$  film (100 at. %), an argon matrix containing 10 vol %  $N_2$ , and a similar matrix containing 5 vol %  $N_2$ . Only losses associated with the vibrational quantum numbers  $v=5-8$  are shown. (b) Mathematical simulation of the spectra in (a).

small coverages, followed by a change in slope and a saturation of current intensities at larger thicknesses. For the broad progression the number of monolayers necessary to produce saturation of the peak height is proportional to the vibrational quantum number. This reflects the increase in the number of multiple collisions with increasing film thickness. The variation in the integrated current distribution of the  $v=1$  peak as a function of the average number of monolayers in the film is shown in Fig. 5. Since multiple phonon losses are included in the range of integration, their effect can be considered as taking part in the elastic collision process. This curve can then be analyzed in terms of one inelastic scattering probability combined with multiple elastic scattering. It has been found, through expression (26) of Ref. 11 applied to a semi-infinite medium, that the intensity of the inelastic current, originating from a single inelastic probability in the multiple scattering regime, was practically constant over a wide range of values of the elastic probability. The remark was also made<sup>11</sup> that the first term in expansion

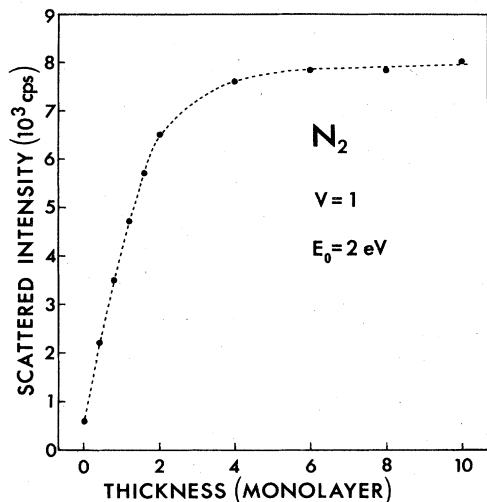


FIG. 5. Intensity of energy losses to the fundamental frequency of  $N_2$  as a function of film thickness for an angle of incidence of  $14^\circ$ .

(1) for a single-collision-related current can be extended to include multiple elastic collisions by renormalizing the sum of total scattering probabilities  $\alpha$ . As an example, the renormalized value of  $\alpha$  may be taken, to a good ap-

proximation, as  $\alpha_i$  (i.e., the sum of the total inelastic scattering probabilities) when the total elastic probability is less than 50% of the sum of the total. For higher values, such as 80% of  $\alpha$ , for the sum of the quasielastic and elastic scattering probabilities, which correspond to our previous estimates at 3 eV for solid  $N_2$ , one can calculate<sup>11</sup> the renormalized  $\alpha$  to be equal to  $1.17\alpha_i$ . For our particular case, this may have the following physical interpretation. If we look at the  $v=1$  peak integrated over a given energy range, only collisions that either take electrons out of the energy range of integration or out of the film contribute to a change in the magnitude of the  $v=1$  intensity with thickness. Thus, since quasielastic multiple scattering is integrated under the  $v=1$  peak in our experiment, only inelastic vibrational excitation and backscattering into vacuum contributes to the sum of the effective total collision probability per unit length which produces the curve in Fig. 5.

With these arguments we may approximate the behavior of the curve in Fig. 5 by the three-dimensional formula (6) in Ref. 11 for the current related to a single-collision process, and in which  $\alpha(E)$  is properly renormalized. For electrons incident at an angle  $\theta_0$  from the film normal with an energy  $E_0$ , with the renormalized  $\alpha(E)$  equal to  $c\alpha_i(E)$ , this formula reads

$$I_1(\theta_0, \theta_d, E) = \frac{I_0 Q (\pi - \theta_0 - \theta_d, E_0, E - E_0)}{\cos \theta_d [c\alpha_i(E_0)/\cos \theta_0 + c\alpha_i(E)/\cos \theta_d]} \left\{ 1 - \exp \left[ - \left( \frac{c\alpha_i(E_0)}{\cos \theta_0} + \frac{c\alpha_i(E)}{\cos \theta_d} \right) L \right] \right\}, \quad (2)$$

where  $\theta_d = \pi - \theta$  is the analyzed backscattering angle and  $E - E_0$  is the energy loss. For small thicknesses, where the exponential term in this formula can be represented by only the first two terms of its Taylor series, we have

$$I_1(\theta_0, \theta_d, E) = \frac{I_0}{\cos \theta_d} Q (\pi - \theta_0 - \theta_d, E_0, E - E_0) L,$$

i.e., the single-collision intensity becomes directly proportional to the thickness when the average inelastic collision number [i.e.,  $\alpha_i(E_0)L/\cos \theta_0 + \alpha_i(E)L/\cos \theta_d$ ] is much smaller than 1. For large values of  $L$  the exponential term tends toward zero, giving

$$I_1(\theta_0, \theta_d, E) = \frac{I_0 Q (\pi - \theta_0 - \theta_d, E_0, E - E_0)}{\cos \theta_d [c\alpha_i(E_0)/\cos \theta_0 + c\alpha_i(E)/\cos \theta_d]},$$

and a saturation in peak intensity is expected. These two behaviors are delineated by a region in Fig. 5 where the slope changes rapidly. This region is characterized by an inelastic collision number close to 1 and *does not necessarily differentiate between monolayer and multilayer regimes*. We can take advantage of this change of slope to estimate the sum of the total vibrational cross section. Then, equating the low- and high-thickness behavior of formula (2) with the approximation  $\alpha_i(E_0) \simeq \alpha_i(E) = nQ_T$ , where  $n$  is the density of molecules in the solid and  $Q_T$  is the total vibrational cross section, we have

$$Q_T = (1/cnL) [(1/\cos \theta_0) + (1/\cos \theta_d)]^{-1}.$$

A value for  $nL$  is obtained by multiplying the number of monolayers (1.5) deduced graphically from Fig. 5 at the intersection of the extrapolation of the low- and high-thickness behavior by the number of molecules in a monolayer. We consider a monolayer from the closed-packed (111) face of the face-centered-cubic crystal structure of  $\alpha$ - $N_2$ .<sup>20,21</sup> This gives  $7.2 \times 10^{14}$  molecules/cm<sup>2</sup>. With  $\theta_0 = 14^\circ$ ,  $\theta_d = 45^\circ$ , and  $c$  taken according to our previous estimate as 1.17, the sum of the total vibrational excitation cross section in the solid at 2 eV is estimated to be  $3.3 \times 10^{-16}$  cm<sup>2</sup>.

When the scattering of an electron with a molecule such as  $N_2$  is dominated by a negative-ion intermediate state, the vibrational excitation amplitude depends on the coherently summed product of Franck-Condon factors allowed between the ground-state  $N_2$  and the  $N_2^-$  state, and those between  $N_2^-$  and the final vibrational states. As shown by the "boomerang" model<sup>38</sup> and several displaced oscillator models,<sup>39</sup> the intensity and periodicity of the oscillatory structure in the cross section are characterized by the lifetime and vibrational spacing energy of the intermediate state. Hence, since the oscillatory structure of the  $N_2^-$  state appears to be similar<sup>8</sup> in the solid and the gas, we expect vibrational cross sections to be about the same in both phases.<sup>38</sup> It is therefore not surprising to find the sum of the total vibrational excitation cross sections for levels  $v=1-8$  in the gas<sup>35</sup> (i.e., about  $7 \times 10^{-16}$  cm<sup>2</sup> at 2.5 eV) to be in good agreement with the value of  $3.3 \times 10^{-16}$  cm<sup>2</sup> estimated from Fig. 5.

Contrary to vibrational excitation, which is enhanced at specific energies, quasielastic losses (i.e., translational plus librational phonons) appear to maintain a strong scattering cross section ( $\approx 5 \times 10^{-16} \text{ cm}^2$ ) throughout the entire (2–20)-eV range. Any dipole excitation would have to arise via the  $2T_u$  translation modes at  $49\text{--}69 \text{ cm}^{-1}$  belonging to the  $Pa3$  structure<sup>36</sup> of  $\alpha\text{-N}_2$ . Most of these modes would be destroyed in our Ar matrices since the barrier-hindering rotation of  $\text{N}_2$  in solid Ar is only  $30\text{--}50 \text{ cm}^{-1}$  ( $3.75\text{--}6.25 \text{ meV}$ ).<sup>40</sup> It would then be difficult, if not impossible, to reproduce the experimental curves by adding only acoustic phonons from the Ar matrix in the calculation without injecting higher-energy rotational modes. We therefore do not expect the  $2T_u$  modes to contribute significantly to energy losses. Hence, it appears difficult to explain the magnitude of the cross section by invoking a dipole mechanism. It is important to realize that at low impact energies, the exchange and quadrupole forces as well as the anisotropic part of the polarization potential can provide an efficient mechanism for exciting librational modes, despite the short range of these interactions. Close-coupling calculations<sup>41</sup> give values of about  $5 \times 10^{-16} \text{ cm}^2$  for the sum of all rotational cross sections at 10 eV in gaseous  $\text{N}_2$ . This value is the same as that obtained for quasielastic losses from our analysis.

The  $2\Pi_g$  resonance recorded with film thicknesses of 2, 4, and 8 ML (ML denotes monolayers) at  $45^\circ$  primary beam incidence in the  $v=1$  decay channel is shown in Fig. 6. Since  $\text{N}_2$  has no permanent dipole moment, the inelastic scattering cross sections are expected to be very small below and above the resonance energy. This may explain the very low scattering intensities seen in Fig. 6 below about 0.8 eV. Above the resonance energy (i.e.,  $E_0 > 4 \text{ eV}$ ) the intensity does not drop to near zero level, possibly because of tailing of the resonance and overlapping with another resonance at 8 eV.<sup>7</sup> The oscillatory structure which modulates the broad maximum centered at 2 eV in Fig. 6 is due to vibrational motion of the two nitrogen atoms in the anion configuration.<sup>8</sup> The shift of the first peak in the upper curve from 1.93 eV in the gas to 1.23 eV in the film determines the value of 0.7 eV for the relaxation shift. The oscillatory structure of  $\text{N}_2^-$  is not observable below thicknesses of about 2 ML. The visibility of the oscillatory structure increases until a thickness of about 8 ML is reached. Referring to Fig. 5, this latter thickness corresponds to saturation of the  $v=1$  vibrational peak intensity and, consequently, to conditions where collisions occurring almost exclusively away from the metal-solid interface contribute to the measured intensity. Hence, it appears that inelastic scattering near the metal-solid interface causes the broadening of the oscillatory structure seen in Fig. 6. This broadening may, *a priori*, originate from a loss in primary energy resolution in the film or from a reduction in the lifetime of the negative ion. This latter effect is usually attributed to a distortion of the centrifugal barrier,<sup>7,8,10</sup> which tends to reduce the symmetry of the negative ion<sup>7,8</sup> and a screening by the metal of the long-range single-electron-molecule polarization potential.<sup>10</sup> It is expected to occur predominantly at monolayer and submonolayer coverages where the attrac-

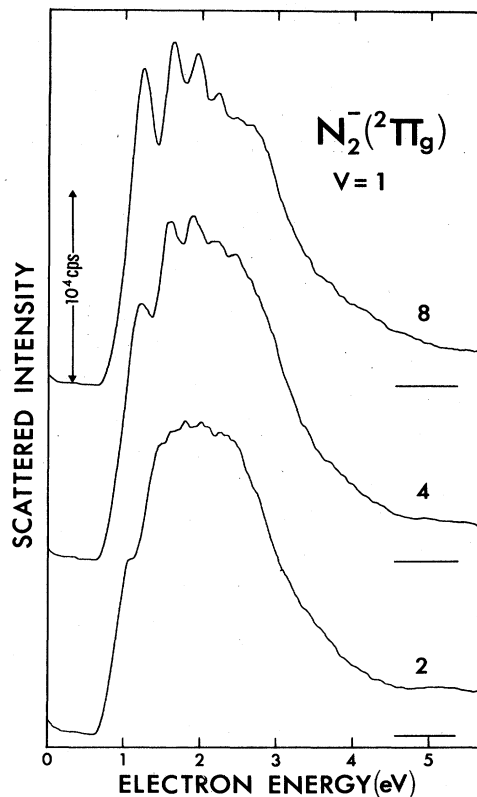


FIG. 6. Vibrational structure of the  $\text{N}_2^-$  temporary anion for films composed of 2, 4, and 8 monolayers (ML). The horizontal base lines on the right-hand side represent the zero intensity for each curve.

tive potential between the anion and its image in the metal and the possible exchange with metal electrons primarily affect the molecular antibonding  $\pi^*$  orbital of the anion.

For monolayer experiments the metal-anion interaction is characterized by a lowering of 0.6 eV in the resonance position with respect to the multilayer-film value and a complete disappearance of oscillatory structure. Above 4 ML, the energy of the resonance does not change appreciably (e.g., by 0.05 eV for the first three peaks upon going from 4 to 8 ML). Consequently, it seems that, above 4 ML, the image force and the shorter-range exchange interaction with the metal has only a small influence on the molecular orbital energies of the anion. We can therefore speculate that contributions to the broadening of the oscillatory structure for 8 ML shown in Fig. 6 results from a loss of primary beam resolution due to fluctuations of potential in the local environment of each molecule. This would be partly caused by the different orientations of  $\text{N}_2$  microcrystals, by the influence of the metal-surface patch fields<sup>42</sup> into the dielectric film, and by changes in the polarization energy of the negative ion due to variation in the number of polarizable neighbors at different depths. If formed in the topmost layer, a negative ion has fewer neighbors and therefore polarizes fewer molecules than when created in the bulk, where it is completely surrounded by neighbors. Its energy is highest at the surface of the film. Thus the contribution from the polarization energy in the relaxation shift is only an average value for both

bulk and surface. This averaging necessarily introduces a broadening in the width of the vibrational structure of the anion. Considering these different contributions, the anion lifetime of  $3 \times 10^{-15}$  sec derived from measurement of the half width at half maximum of the first vibrational peak<sup>8</sup>, can only be taken as a lower limit. In any case, this figure should be considered an estimate since a proper determination of the lifetime would also require analysis of the amplitude of the vibrational structure in different decay channels using a displaced oscillator model.<sup>38,39</sup> These models may be more easily applicable to submonolayer experiments where multiple librational collisions are significantly reduced. A twice-displaced oscillator model has recently been used by Gadzuk<sup>39</sup> to estimate the lifetime broadening induced by the metal surface in the experiment of Schmeisser *et al.*<sup>10</sup> From the amplitude of the vibrational peak, he finds<sup>39</sup> the lifetime of the  ${}^2\Pi_g$  state of  $N_2^-$  to be reduced 40% from its gas-phase value at submonolayer coverage.

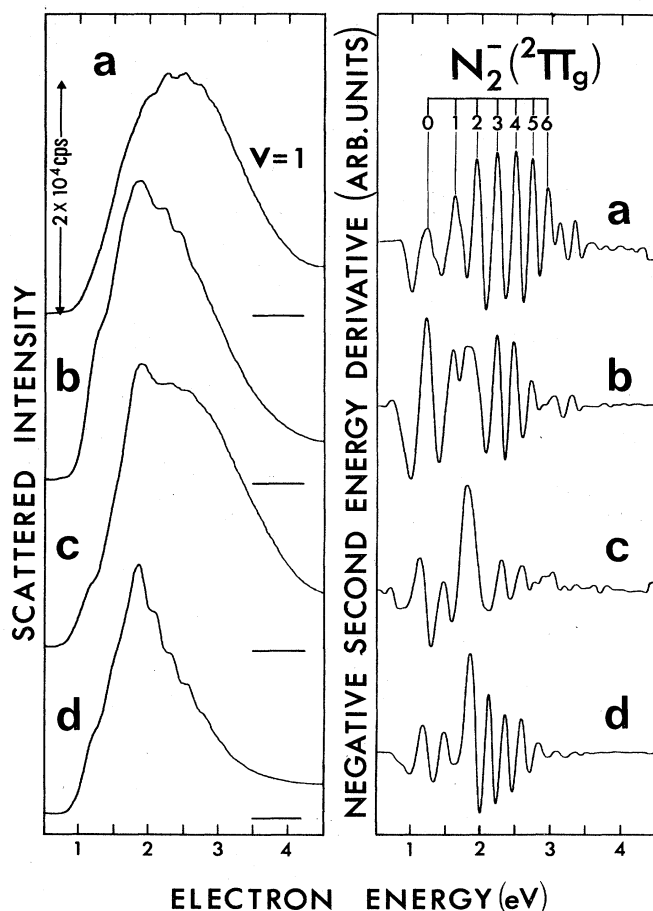


FIG. 7. Line shape and vibrational structure of the  $N_2^-$  ( ${}^2\Pi_g$ ) temporary state for 8-ML films composed of *a*, disordered  $N_2$  crystallites; *b*,  $N_2$  crystallites covered by a film of Ar having the same thickness; *c*, Ar covered by a film of  $N_2$  crystallites having the same thickness; and *d*, Ar containing 10 vol %  $N_2$ . The negative value of the second energy derivative of curves *a*–*d* on the left-hand side is shown on the right-hand side. The oscillatory structure which appears modified by the surrounding medium is due to the nuclear motion of the anion.

Deterioration of primary beam resolution caused by inhomogeneities of local potentials in disordered crystals of  $N_2$  is exemplified by curves *a*–*d* on the left-hand side of Fig. 7. Each curve represents the excitation function of the fundamental vibrational level of ground-state  $N_2$  in an 8-ML film for (*a*) a highly disordered  $N_2$  film, (*b*) a film of  $N_2$  covered by a film of Ar having the same thickness, (*c*) a similar film of Ar covered by a  $N_2$  film, and (*d*) a Ar film containing 10 vol % of  $N_2$  molecules. All other parameters are the same as those needed to produce the top curve in Fig. 6. The lower degree of order in these films causes the vibrational structure of the anion to be barely perceivable. In order to demonstrate that these weak undulations are effectively due to nuclear motion of  $N_2^-$ , the negative value of the second energy derivative of curves *a*–*d* is displayed on the right-hand side of Fig. 7. Each maximum would correspond to the position of a vibrational level  $N_2^-$  if the anion had sufficient time to vibrate during its lifetime. During  $3 \times 10^{-15}$  sec,<sup>8</sup> there is not sufficient time for the nuclear wave function to fully develop and the oscillatory structure does not truly represent vibrational levels, even though a strong anharmonicity is clearly apparent in curves *a* and *d*. According to the "boomerang model,"<sup>38</sup> changes in the lifetime of the anion would also influence the relative energy of each maxima in the doubly differentiated curves of Fig. 7. Experimentally, these maxima retain the same relative position (within  $\pm 0.01$  eV) for ordered or disordered films, providing evidence that the major broadening influences in multilayer films are essentially due to potential fluctuations.

Since the resonance interaction is most likely to be localized on a single molecule,<sup>8</sup> we do not expect the vibrational-librational excitation cross sections to change appreciably in the different films. The changes in line shapes and amplitudes are therefore believed to result from changes in the elastic mean free path (MFP), and may serve as an example to illustrate how this parameter can affect electron-energy losses. Its effect is obvious from formula (2): if  $Q$  is constant and the thickness  $L$  much larger than the total MFP, the contribution from single collisions to the intensity of an energy-loss peak is essentially inversely proportional to the parameters  $\alpha_i(E_0)$  and  $\alpha_i(E)$ , which contain in  $c$  the elastic collision probability before and after the inelastic encounter, respectively. As an example, we can discuss the differences between spectra *a* and *d* in Fig. 7. According to formula (2) the steep decrease in scattered intensity above 2 eV in *d* would result from a strong increase in the total scattering probability. In fact, we do find from electron transmission experiments<sup>43,44</sup> that above 2 eV the elastic MFP in the solid rare gases is reduced by more than an order of magnitude. Below 2 eV, elastic MFP's can reach values as high as 250 Å,<sup>43</sup> so that in the (1–2)-eV range, we observe, as expected, a larger amplitude in curve *d* than in curve *a* and the inverse above 2 eV. Another factor which probably tends to diminish the elastic MFP is the higher disorder in the matrix compared to the pure- $N_2$  film. Over- or under-covering an  $N_2$  film with Ar layers not only changes the amplitude and line shape of the resonance, but also perturbs its vibrational structure, as seen

in curves *b* and *c* on the right-hand side of Fig. 7.

Variation in the resonance profile as a function of angle of incidence between  $15^\circ$  and  $45^\circ$  from the normal is shown on the left-hand side of Fig. 8. The data were recorded in the  $\nu=1$  decay channel of  $N_2$  in a pure film  $50 \text{ \AA}$  thick. The amplitudes of the first, second, and third vibrational peaks of the resonance, measured at incident energies  $E_0=1.2, 1.6,$  and  $1.9 \text{ eV}$ , respectively, are shown as a function of angle of incidence on the right-hand side of the figure. The distribution for all three peaks has a maximum around  $40^\circ$ , which corresponds to a scattering angle of  $85^\circ$  between the directions of the primary and scattered beams.

The  ${}^2\Pi_g$  state of  $N_2^-$  is formed by adding an electron in the lowest unfilled  $\pi_g$  orbital of ground-state  $N_2$ . Spherical-harmonic expansion of the electron wave function for that orbital indicates that the angular momentum of the detaching electron must have a strong *d*-wave ( $l=2$ ) character. For uncorrelated randomly oriented molecules, the *d*-wave behavior of the cross section for various vibrational states of  $N_2$  is therefore expected to show a peak at a scattering angle near  $90^\circ$ . This behavior seen in Fig. 8 has been previously observed in the gas phase by Ehrhardt and Willmann<sup>32</sup> in various decay channels, and by Tanaka *et al.*<sup>45</sup> in the  $\nu=1$  channel. For a range of scattering angles corresponding to a change from  $15^\circ$  to  $45^\circ$  angle of incidence in our experiments, the absolute differential cross section for the  $\nu=0 \rightarrow 1$  transition

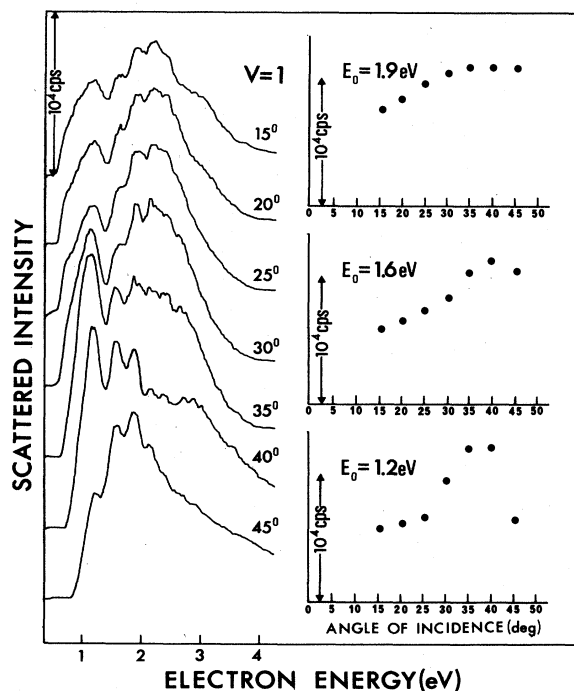


FIG. 8. Line shape and vibrational structure of the  $N_2^-$  ( ${}^2\Pi_g$ ) temporary anion for different angles of incidence of the primary beam ( $15^\circ$ – $45^\circ$  with respect to the normal of a  $50\text{-\AA}$ -thick film) is shown on the left-hand side. The angular distribution for the intensity of the first three peaks in the oscillatory structure, occurring at 1.2, 1.6, and 1.9 eV, respectively, is shown on the right-hand side.

in the gas changes by about a factor of 2. At 1.2 eV incident energy, we find about the same factor, but at higher primary energies the maximum near  $40^\circ$  is less pronounced. The *d*-wave behavior of the resonance also appears less pronounced at higher impact energies in gas-phase work, but this is probably due to changes in *l*-wave admixture. However, in the solid the effect is more intense and we may conjecture that multiple scatterings have a tendency to wash out the maximum near  $40^\circ$ . According to formula (2) the angular distribution should be directly proportional to the differential scattering cross section, but this relationship neglects multiple collisions, such as librational energy losses, which can change the scattering angle before and after excitation of the  $\nu=1$  state. It is also possible that the partial-wave content of the outgoing wave is different in the solid, thus modifying gas-phase angular distributions. As shown by the calculation of Davenport *et al.*,<sup>46</sup> orientating the molecule on a surface can modify the amplitude and shape of the angular distributions. In the case of orientated  $N_2$  the shape of the angular distribution is independent of incident direction.<sup>46</sup> The intensity maximum occurs at  $45^\circ$  angle of incidence relative to the molecular axis and vanishes with incidence either on the axis or perpendicular to the axis.

#### B. Carbon monoxide

Energy-loss spectra recorded in  $50\text{-\AA}$ -thick CO films at a  $14^\circ$  angle of incidence from the normal are shown in Fig. 9. The curves at the top, middle, and bottom correspond to primary energies of  $E_0=2.5, 5,$  and  $20 \text{ eV}$ , respectively. The insets show the  $E_0=2.5$  and  $5 \text{ eV}$  data when recorded in the specular direction at  $45^\circ$  incidence. The gain given to each curve or portion of a curve is referenced to the elastic peak at the top left-hand side of the figure. The strong enhancement of overtones of the fundamental frequency at  $E_0=2.5 \text{ eV}$  is due to the formation of the ground-state anion with molecular parcentage  ${}^2\Pi$ . At  $20 \text{ eV}$ , overtone frequencies can still be perceived, possibly due to the formation of another higher-lying state of  $CO^-$ . The  $\nu=1$  peak is also enhanced by the resonance, but its angular dependence is different from that of  $\nu=2$ . In going from  $14^\circ$  to  $45^\circ$ , the intensity of the  $\nu=1$  peak is increased by a factor of 4, 5, and 10 at 2.5, 5, and 8 eV, respectively, in comparison with a factor of 2 for the  $\nu=2$  level at 2.5 eV. Concurrently, the elastic beam is about 20 times stronger in the specular direction. Since the CO molecule, contrary to  $N_2$ , possesses a permanent dipole, we must take into account the additional contribution to vibrational excitation mainly due to the change of dipole moment with internuclear distance. Within the scattering theory of slow electrons by a long-range dipole interaction<sup>47</sup> with ordered molecules sitting on or forming a reflecting surface, we expect contributions to the inelastic scattered intensity to occur only in the specular direction. In the present experiment, however, our films are composed of disoriented polycrystals. Long-range scattering can therefore occur at angles other than at  $45^\circ$  incidence.

Off resonance (i.e., at  $E_0=5 \text{ eV}$ ), in the specular direction, the low intensity of the overtones, in comparison

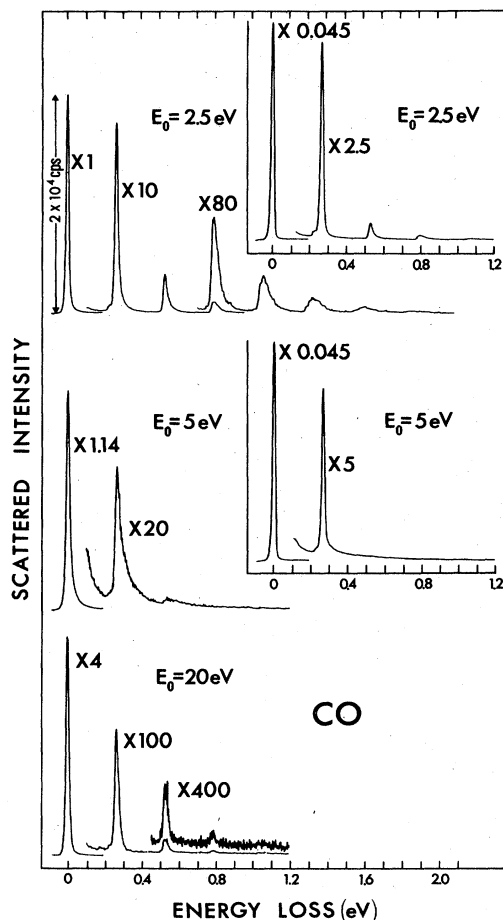


FIG. 9. Energy-loss spectra for 2.5-, 5-, and 20-eV electrons impinging on a 50-Å-thick CO film. The curves shown in the insets were recorded in the specular direction. The others were recorded with a beam incident at  $14^\circ$  from the surface normal. The gain in each curve is referenced to the "elastic" peak in the top left-hand tracing.

with the amplitude of the  $v=1$  peak, indicates that the selection rule<sup>47</sup>  $\Delta v=1$  holds, to a certain extent, and that multiple collisions of dipolar origin do not contribute significantly to the spectra. By comparing the different ratios found experimentally, we can estimate the dipolar contribution to the inelastically scattered intensity at  $E_0=2.5$  eV to be about 50% at  $45^\circ$  and 15% at  $14^\circ$ . Here, because of the low value of the dielectric constant of the film, no cancellation of the contribution due to the component of the dipole parallel to the surface is expected to take place, contrary to the case of an isolated molecule on a metal surface.<sup>26</sup> The amplitude of long-range dipole scattering should therefore not be strongly dependent on the orientation of the normal modes of the molecules with respect to the surface, making a molecular orientational study based on this particular image dipole selection rule ineffective.

The general trend of the energy-loss spectrum of CO at  $E_0=2.5$  eV is similar to that observed in  $N_2$ , but no sharp progression can be resolved. It is composed of a series of peaks of increasing FWHM and decreasing amplitude

with energy loss. These peaks exhibit no measurable anharmonicity. Calculations of the energy-loss spectrum from multiple scattering theory indicate that they result from a combination of multiple and single collisions broadened by phonon losses, as in the case of  $N_2$ . Pure rotational excitation measurements<sup>33</sup> in the gas phase yield even stronger cross sections for CO than  $N_2$  in the region of the  $^2\Pi$  resonance. Here again, if we have a situation where probabilities of librational excitations can be associated with rotational cross sections, librations may still be the major contribution to the CO phonon spectrum. Rotational excitation is still strong off resonance in CO gas.<sup>48</sup> The disappearance of single-loss peaks in the solid may therefore be due to the overall higher librational energy loss in CO than in  $N_2$ . Another mechanism which can enhance electron-phonon coupling in CO films is the interaction of the negative-ion state with the dipole-active intermolecular or intramolecular modes of surrounding molecules via long-range Coulomb forces. The consequences of this type of interaction have been described by a generalization of the Huang-Rhys model<sup>49</sup> and applied, so far, to interpret x-ray spectra of alkali halides<sup>50</sup> and uv photoelectron spectra.<sup>51-53</sup> The theory should be applicable to interpret negative-ion-phonon coupling in a similar manner as for hole-phonon coupling in photoemission. However, the short lifetime of transient anions ( $\sim 10^{-15}$  sec), compared to the vibrational period of the phonons modes ( $10^{-12}$  sec), should reduce the energy transferred.

Off resonance, the vibrational cross sections decrease, and multiple vibrational collisions are much less prominent. Phonons become the major energy-loss mechanism. As explained for  $N_2$ , they can cause an unusually large broadening of the vibrational peaks when they dominate inelastic processes. This is shown in Fig. 9 where we find a value of 35 meV for the FWHM of the  $v=1$  level at  $E_0=5$  eV (i.e., off resonance), compared to the value of 18 meV at  $E_0=2.5$ . We also note that in the specular direction at  $E_0=5$  eV the elastic and  $v=1$  peaks are much less broadened. These peaks arise mainly from coherently scattered waves which, necessarily, have little inelastic multiple interactions with the target. At 20 eV, phonon broadening also occurs (with a FWHM of about 23 meV for  $v=1$ ), but multiple vibrational losses are suppressed by the occurrence of electronic transitions. The  $v=1-4$  peaks in the spectrum at the bottom of Fig. 9 exhibit an anharmonicity ( $\omega_e x_e=3$  meV) similar to gas-phase<sup>28</sup> CO.

The angular distribution of the resonant part of the scattered distribution depends on the symmetry of the negative ion. The  $^2\Pi$  resonance in CO has a lower symmetry than in  $N_2$  which results in a partial-wave expansion for resonant electrons with mainly  $p$ - and  $d$ -wave contributions. Owing to interference between these two waves, the angular patterns and intensities for resonant vibrational excitation from orientated molecules are strong functions of the direction of incidence.<sup>46</sup> Irrespective of the dipole contribution, we find the strongest enhancement for the overtones near  $45^\circ$ , as predicted by theory,<sup>46</sup> for CO molecules sitting with their axis perpendicular to the surface.

The excitation function for  $v=1-3$  measured at a  $14^\circ$  angle of incidence is shown in Fig. 10(a) along with the energy dependence of the "quasielastic" peak (i.e.,  $v=0$ ). Measurements taken at  $45^\circ$  incidence are shown in Fig. 10(b), the inset. The strong increase in the vibrational intensities having a maximum at  $(2.25 \pm 0.15)$  eV is interpreted as resulting from the formation of a temporary anion with molecular parentage  $^2\Pi$ . Another broad "hump" centered around 19 eV is present in all vibrational excitation functions. It probably results from the formation of another transient ion with a resonant electron having a higher-order angular momentum partial-wave content. From comparison with the similar isoelectronic  $N_2^-$  state, the molecular parentage of the solid-phase anion would be  $^2\Sigma$ . A similar resonance has been observed near 22 eV in gaseous CO, but, at the time, the state was interpreted as arising from many doubly excited states.<sup>54</sup> As expected, the  $^2\Sigma$  state lies at lower energy in the solid than in the gas phase. Since we do not observe the oscillatory structure of the gas-phase  $^2\Pi$  anion, it is difficult to make such energy comparison with the 2.25-eV maxima.

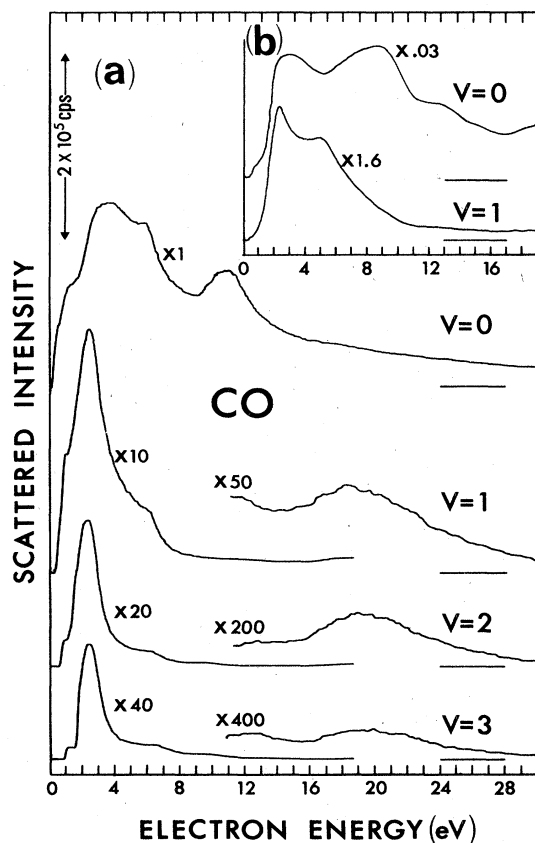


FIG. 10. (a) Energy dependence of quasielastic peak ( $v=0$ ) and vibrational energy losses ( $v=1-3$ ) recorded at a  $14^\circ$  angle of incidence in a CO film. The broad "humps" in the excitation functions result from the formation of transitory  $CO^-$  states. (b) Same as (a) but recorded in the specular direction (i.e., at  $45^\circ$  incidence). The horizontal bars at the end of each spectrum denote the zero-intensity baseline.

The small-amplitude sharp peak near 6 eV in Fig. 10 is present at all scattering angles except in the elastic specular beam [top curve in inset, (b)]. Hence, it cannot be associated with the off-specular reflectivity. Its presence in the  $v=0$  curve indicates that it probably occurs in the phonon excitation function, which cannot be resolved from that of purely elastically scattered electrons. From our multiple scattering calculation, the measured intensity of the  $v=0$  function in the (4–7)-eV region would be composed mainly of electrons which have suffered multiple librational losses. Any structure present in phonon excitation functions could therefore be reproduced in all observable channels, including  $v=0$ . In the specular direction, the amplitude of the wave function is governed by coherent elastic scattering, and quasielastic effects are more difficult to observe. A peak around 7 eV in the excitation function of  $N_2$  films has been ascribed<sup>7</sup> to a shape resonance whose symmetry has not yet been determined.<sup>3</sup> It is possible that a similar state could explain the 6-eV peak in CO. However, the width of this peak is much sharper in solid CO (FWHM of about 0.5 eV) than in  $N_2$  films (FWHM of about 1.9 eV). On the other hand, sharp structure has been observed<sup>55</sup> in the elastic and vibrational ( $v=1$  and 2) cross sections of the ground electronic state of gaseous CO at energies coincident with the  $v=0, 1$ , and 2 levels of the  $a^3\Pi$  state of CO at 6 eV. This feature was not related to a single-particle shape resonance, but was rather interpreted as arising from a core-excited resonance produced by the binding of an incoming electron by the dipole moment (1.38 D) (Ref. 56) of the  $a^3\Pi$  state of CO. In such a "dipole-dominated" resonance the projectile electron is trapped near the top of the potential well of the  $^3\Pi$  state, which is highly asymmetrical.<sup>55</sup> Its temporary localization could therefore exert considerable torque on the CO molecule and efficiently transfer rotational or librational energy. The 6-eV structure in Fig. 10 is therefore likely to be due to the formation of a dipole-dominated resonance. Structures related to other gas-phase core-excited resonances<sup>57</sup> were not detected.

The sharp increase near 1 eV in the intensity of the  $v=1-3$  vibrational levels [Fig. 10(a)] results from the onset of the nonresonant part of the excitation function on which the strong maxima at 2.5 eV is superimposed. Although relatively less pronounced in the  $v=2$  and 3 channels, the nonresonant part of the excitation function, which contains the dipole and the remaining part of the short-range scattering contributions, still exists.

The variation in the amplitude of the  $v=2$  excitation function with coverage is shown in Fig. 11. The approximate number of monolayers is indicated on top of each curve. We note four salient features in these curves: the energy of the  $^2\Pi$  resonance increases up to about 3 ML and then remains constant, its amplitude increases rapidly up to about 3 ML, the ratio of the amplitudes of the nonresonant to the resonant contribution is greater at submonolayer coverage, and the energy onset of the nonresonant contribution is independent of coverage. The lowering by 0.7 eV of the  $^2\Pi$  resonance at submonolayer coverage is attributed to a breakdown in symmetry and screening of the charge by the metal. Energy derivatives of the spectra in Fig. 11 did not reveal vibrational struc-

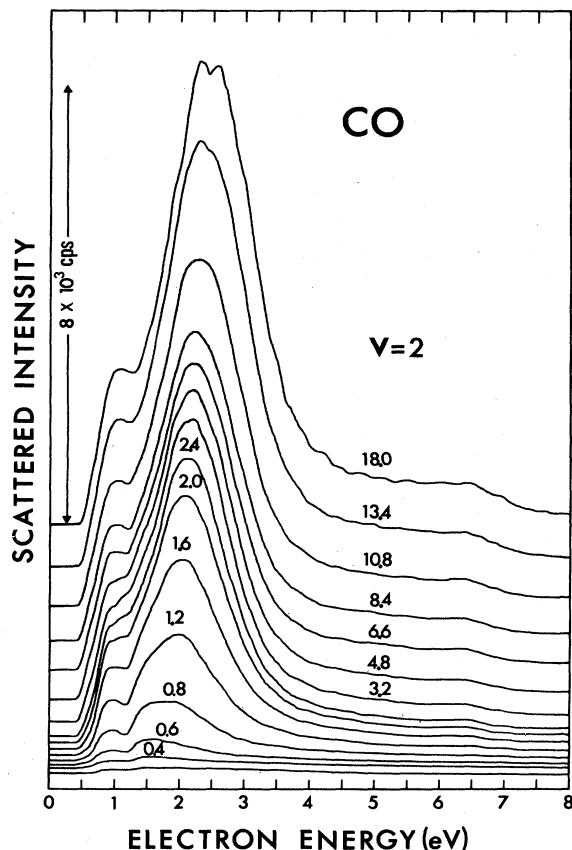


FIG. 11. Excitation function of the  $v=2$  vibrational level of CO recorded at film thicknesses ranging from 0.4 to 18 ML. The strong peak having a maximum near 2 eV is due to the formation of a  ${}^2\Pi$  state of  $\text{CO}^-$ .

ture in the  ${}^2\Pi$  state of  $\text{CO}^-$ . As in the case of  $\text{N}_2$ , we expect little change in the electronic configuration of the anion in the solid. The disappearance of the gas-phase vibrational structure may therefore arise from fluctuations of local potentials due to disorder in the films. The vibrational structure of the  ${}^2\Pi$  state in CO gas is already broader (0.4 eV) (Ref. 58) than that in  $\text{N}_2$  gas. Additional broadening influences in our film may therefore completely wash out the oscillatory structure.

#### C. Relaxation energy of transient negative ions

The total "relaxation energy" of a transient negative ion, or energy difference between the anion energy in the gas and that in *multilayer* solid film,<sup>5,7,8</sup> may be divided into two components originating from intramolecular and extramolecular forces. Energy changes due to extramolecular relaxation not only result from the screening of the negative charge by the polarization of the surrounding molecules, but also from the influence of the surrounding matrix on the anion molecular orbital configuration. The latter shift is similar to the chemical shift observed in photoemission. If the interaction of surrounding mole-

cules with the negative ion is strong (e.g., if the wave function of the extra electron strongly overlaps with neighbors), we may expect the anion to reduce its molecular symmetry or even lose its identity. A breakdown in the molecular symmetry of a transient anion will automatically modify the partial-wave content of the spherical-harmonic expansion of the resonant electron wave function. The lower symmetry is most likely to result in a wave packet containing more spherical harmonics of lower angular momentum. Thus, the extra electron can tunnel more easily through its centrifugal barrier, and the energy and the lifetime of the anion are reduced. If the configuration interaction is small, the energy shift will result mainly from screening, but its magnitude may depend on the lifetime of the transient state since the polarization of the medium is related to the time of residence of the electron at a particular molecular site. For short-lived anions ( $< 10^{-15}$  sec) the localization time may be too short to allow complete electronic polarization of the surrounding medium. In this case, the intramolecular relaxation related to reorganization of the electronic orbital of the negatively charged molecule may also be incomplete. Thus, when the lifetime changes from gas to solid, the total relaxation energy could also be modified via the intramolecular relaxation-energy term. We also note that when the MFP is small, electrons interact with the first few layers of the film. Consequently, the contribution of the polarization energy to the measured relaxation shift is smaller than that in the bulk due to the reduction of polarizable nearest neighbors in the vicinity of the surface.

#### D. Influence of electron-energy losses in the photoelectron spectra of multilayer molecular films

In a three-step model the emission intensity of photoelectrons from a multilayer film deposited on a metal surface depends essentially on the transition of an electron from an occupied molecular state to an unoccupied state above the vacuum level, on the transmission function of the photoelectron from the site of creation to the film-vacuum interface, and, finally, on the reflection coefficient at this interface. The transmission function is strongly dependent on the electron inelastic MFP, and we therefore expect the intensity, energy, and linewidths of the photoelectron structures to be influenced by librational and vibrational electron scattering. Inelastic MFP's of the order of a few angstroms, such as those determined here for  $\text{N}_2$  and CO, are bound to strongly attenuate the number of emitted photoelectrons. As an example, we may cite the results of Lau, Foch, and Koch,<sup>59</sup> who studied the amplitude of the photoelectric signal from a multilayer  $\text{N}_2$  film as a function of photoelectron energy using a variable-energy photon source. They observed a strong depletion of the photoelectric yield for a departing electron of about 2 eV energy in  $\text{N}_2$ .

Multiple librational and vibrational energy losses by photoelectrons will necessarily also contribute to the energy spread of the spectral features in solid-phase photoemission. Several mechanisms<sup>52,53,60</sup> have been proposed to explain the broadening of photoemission lines of con-

densed multilayer experiments, especially in connection with the work<sup>60,61</sup> in N<sub>2</sub> and CO. It appears that the initial hole lifetime does not contribute to the level width, and that smearing due to hole-phonon coupling is insufficient to explain the observed widths. The remaining explanations which seem plausible include site-to-site variations in local potential, spatial variations in intermolecular relaxation energies in the vicinity of the surface,<sup>62,63</sup> and librational and vibrational energy losses. The latter losses will be particularly effective when low-energy photons are utilized. They should be considerably reduced in rare-gas matrix-isolation experiments and may, at least partly, explain the reduction in photoelectron peak width observed by Schmeisser and Jacobi<sup>60</sup> in matrix-isolated CO and N<sub>2</sub> relative to the condensed multilayer values. Finally, we note that librational and vibrational losses can shift the maxima of photoelectron peaks to lower energies and possibly give values of differences in gas- to solid-phase relaxation energies which are too high.

#### IV. CONCLUSIONS

In this work, we have described some aspects of inelastic electron scattering from solid films composed of N<sub>2</sub> and CO molecules. These included vibrational and librational excitation, multiple scattering effects, and transient anion formation. Since the total scattering cross sections involved in the primary energy range of interest (1–30 eV) are high ( $\approx 10^{-16}$  cm<sup>2</sup>), the target films ( $\approx 50$  Å thick) had to be considered "thick" by the electron beam. It was therefore necessary to resort to multiple scattering theory<sup>11</sup> in order to properly interpret energy-loss spectra. Despite the limitations imposed on the measurements by multiple collisions, it was possible to identify contributions from individual, major energy-loss mechanisms. Energy-loss spectra were composed of peaks which resulted from single and multiple vibrational losses broadened by multiple phonon losses. Phonon distributions consisted essentially of librational modes having energies similar to those found in infrared and Raman spectra, but with much different amplitudes.

By measuring the excitation functions of intramolecular vibrational losses over wide energy limits, it was possible to study the influence of film thickness and order, matrix isolation, and angle of electron incidence on the formation of transient negative ions. In both N<sub>2</sub> and CO, the lowest-energy anion was not appreciably perturbed by surrounding neighbors. The energy of the <sup>2</sup>Π<sub>g</sub> state of N<sub>2</sub><sup>-</sup> relaxed by 0.7 eV in the solid, but the energy of the isoelectronic <sup>2</sup>Π anion in CO appeared to remain the same as in the gas. At submonolayer coverage the resonance interaction still dominated short-range scattering, and both anions relaxed by an additional 0.6–0.7 eV due to in-

teraction with the metal. In addition to the observation of the <sup>2</sup>Π and <sup>2</sup>Σ resonances in CO films, a sharp peak near 6 eV incident energy in the excitation functions could be correlated with a core-excited resonance associated with the dipole field of the <sup>3</sup>Π state.

From measurements of the intensity of the fundamental vibrational loss in N<sub>2</sub> as a function of film thickness, the total cross section for excitation of all possible vibrational levels of N<sub>2</sub> was found to be  $3.3 \times 10^{-16}$  cm<sup>2</sup> at resonance, and the sum of all phonon cross sections was found to be about  $5 \times 10^{-16}$  cm<sup>2</sup>. These cross sections were slightly higher in CO, possibly because of the additional dipole interaction which still contributed to at least 40% of the total  $\nu = 1$  cross section at resonance (i.e., at 2.5 eV impact energy) in multilayer films. This percentage was even higher at submonolayer coverage. The probability of libron excitation, which appeared to dominate the total phonon cross section, remained high throughout the entire (1–20)-eV range, indicating that a resonance mechanism is not necessarily needed to strongly excite these modes (i.e., the short-range exchange and/or quadrupole forces, as well as the anisotropic part of the induced polarization potential, can provide an efficient interaction for exciting librational modes).

In conclusion, we have shown that transient negative ions can provide an efficient mechanism to enhance short-range scattering and the intensity of vibrational overtones, which, in turn, can serve in the derivation of information on adsorbate bonding geometry,<sup>46</sup> vibrational relaxation rates, and dissociation energies.<sup>64</sup> On more fundamental grounds, these anion states may provide a powerful probe to understand low-energy electron interactions in condensed phases and intramolecular multiple scattering in large molecules [e.g., multiple scattering resonances in Fe(CN)<sub>6</sub> complexes<sup>65</sup>]. Since the forces which produce the electron trapping in an isolated electron-molecule system are well understood,<sup>1,3,4,66</sup> their modification by neighboring targets could provide a link to relate some of the abundant knowledge on isolated molecules<sup>1,4,66</sup> to that in other phases. This should be particularly important for techniques where low-energy electrons are involved either as a probe (e.g., electron-stimulated desorption and inverse photoemission) or as a product of the primary interaction (e.g., photoelectric emission).

#### ACKNOWLEDGMENTS

We wish to thank L. Caron and J.-P. Jay-Gerin for stimulating discussions, and G. J. Fisher for his critical evaluation of this manuscript. Financial support from the Medical Research Council of Canada is gratefully acknowledged.

<sup>1</sup>For a review of electron resonances in gases, see G. J. Schulz, *Rev. Mod. Phys.* **45**, 378 (1973); **45**, 423 (1973).

<sup>2</sup>We exclude from this definition shape resonances associated with photoelectron emission.

<sup>3</sup>G. J. Schulz, in *Principles of Laser Plasmas*, edited by G. Bekefi (Wiley, New York, 1976), p. 33.

<sup>4</sup>H. S. W. Massey, *Negative Ions* (Cambridge University Press, London, 1976).

<sup>5</sup>L. Sanche and M. Michaud, *Phys. Rev. Lett.* **47**, 1008 (1981).

<sup>6</sup>J. E. Demuth, D. Schmeisser, and Ph. Avouris, *Phys. Rev. Lett.* **47**, 1166 (1981).

<sup>7</sup>L. Sanche and M. Michaud, *Chem. Phys. Lett.* **84**, 497 (1981).

- <sup>8</sup>L. Sanche and M. Michaud, *Phys. Rev. B* **27**, 3856 (1983).
- <sup>9</sup>L. Sanche and M. Michaud, *J. Chem. Phys.* **81**, 257 (1984).
- <sup>10</sup>D. Schmeisser, J. E. Demuth, and Ph. Avouris, *Phys. Rev. B* **26**, 4857 (1982).
- <sup>11</sup>M. Michaud and L. Sanche, preceding paper, *Phys. Rev. B* **30**, 6067 (1984).
- <sup>12</sup>M. Michaud and L. Sanche, *J. Vac. Sci. Technol.* **17**, 274 (1980).
- <sup>13</sup>E. Harting and F. H. Read, *Electrostatic Lenses* (Elsevier, New York, 1976).
- <sup>14</sup>E. A. Soa, *Jenaer Jahrb.* **1**, 115 (1959).
- <sup>15</sup>B. A. Sexton and G. E. Mitchell, *Surf. Sci.* **99**, 539 (1980).
- <sup>16</sup>Y. C. Chang and W. B. Berry, *J. Chem. Phys.* **61**, 2727 (1974).
- <sup>17</sup>T. E. Madey, *Surf. Sci.* **33**, 355 (1972).
- <sup>18</sup>L. Sanche, *J. Chem. Phys.* **71**, 4860 (1979).
- <sup>19</sup>R. E. Honig and H. O. Hook, *RCA Rev.* **21**, 360 (1960).
- <sup>20</sup>L. Vegard, *Z. Phys.* **79**, 471 (1932).
- <sup>21</sup>L. H. Bolz, M. E. Boyd, F. A. Mauer, and H. S. Perser, *Acta Crystallogr.* **12**, 249 (1959); L. Vegard, *Z. Phys.* **61**, 185 (1930).
- <sup>22</sup>E. M. Horl and L. Marton, *Acta Crystallogr.* **14**, 11 (1961); J. Donahue, *ibid.* **14**, 1000 (1961).
- <sup>23</sup>G. Zumofen, *J. Chem. Phys.* **68**, 3747 (1978); M. Rossinilli, M. Bosch, and G. Zumofen, *Phys. Rev. B* **22**, 6403 (1980).
- <sup>24</sup>F. Legay, N. Legay-Sommaire, and G. Zumofen, *Chem. Phys.* **68**, 437 (1982); J. Klafter and J. Jortner, *ibid.* **71**, 2210 (1979).
- <sup>25</sup>J. O. Clayton and W. F. Giaouque, *J. Am. Chem. Soc.* **54**, 2610 (1932).
- <sup>26</sup>For a review of electron scattering from molecules adsorbed or chemisorbed on metal surfaces, see J. C. Bertolini and J. Rousseau, *Ann. Phys. (Paris)* **5**, 115 (1980).
- <sup>27</sup>L. Sanche, G. Bader, and L. G. Caron, *J. Chem. Phys.* **76**, 4016 (1982).
- <sup>28</sup>G. Herzberg, *Spectra of Diatomic Molecules* (Van Nostrand, Princeton, N.J., 1966).
- <sup>29</sup>J. W. Boness and G. J. Schulz, *Phys. Rev. A* **8**, 2883 (1973), and unpublished.
- <sup>30</sup>M. Brith, A. Ron, and O. Schnepf, *J. Chem. Phys.* **51**, 1318 (1969); J. E. Cahill and G. E. Leroi, *ibid.* **51**, 1324 (1969).
- <sup>31</sup>A. Anderson, T. S. Sun, and M. C. A. Donkersloot, *Can. J. Phys.* **48**, 2265 (1970); P. M. Mathai and E. J. Allin, *ibid.* **49**, 1973 (1971).
- <sup>32</sup>H. Ehrhardt and K. Willmann, *Z. Phys.* **204**, 462 (1967).
- <sup>33</sup>S. F. Wong and L. Dubé, *Phys. Rev. A* **17**, 570 (1978); K. Jung, Th. Antoni, R. Muller, K.-H. Kochem, and H. Ehrhart, *J. Phys. B* **15**, 3535 (1982).
- <sup>34</sup>G. J. Schulz, *Phys. Rev.* **135**, A988 (1964).
- <sup>35</sup>The sum of total cross sections for all vibrational states was estimated from the results of Ref. 34 and by calibrating  $v = 1$  on the rotationally summed value of  $2.0 \times 10^{-16} \text{ cm}^2$  given by Jung *et al.* (Ref. 33) at 2.47 eV incident energy. The value for pure rotational excitation ( $6.8 \times 10^{-16} \text{ cm}^2$ ) was taken from the same authors.
- <sup>36</sup>A. Anderson and G. E. Leroi, *J. Chem. Phys.* **45**, 4359 (1966); A. Ron and O. Schnepf, *ibid.* **46**, 3991 (1967); R. V. St. Louis and O. Schnepf, *ibid.* **50**, 5177 (1969); J. A. Venables and C. A. English, *Acta Crystallogr. Sect. B* **30**, 929 (1974).
- <sup>37</sup>M. Birth, A. Ron, and O. Schnepf, *J. Chem. Phys.* **51**, 1318 (1969); M. M. Thiery, D. Fabre, M. Jean-Louis, and H. Vu, *ibid.* **59**, 4559 (1973).
- <sup>38</sup>D. T. Bertwistle and A. Herzenberg, *J. Phys.* **4**, 53 (1971); L. Dubé and A. Herzenberg, *Phys. Rev. A* **20**, 194 (1979).
- <sup>39</sup>J. W. Gadzuk, *J. Chem. Phys.* **79**, 3982 (1983); W. Domcke and L. S. Cederbaum, *Phys. Rev. A* **16**, 1465 (1977).
- <sup>40</sup>H. Dubost, *Ber. Bunsenges. Phys. Chem.* **82**, 112 (1978).
- <sup>41</sup>D. G. Truhlar, M. A. Brandt, A. Chutjian, S. K. Srivastava, and S. Trajmar, *J. Chem. Phys.* **65**, 2962 (1976).
- <sup>42</sup>C. Herring and M. H. Nichols, *Rev. Mod. Phys.* **21**, 185 (1949).
- <sup>43</sup>G. Bader, G. Peruzzo, L. G. Caron, and L. Sanche, *Phys. Rev. B* **26**, 6019 (1982).
- <sup>44</sup>L. Sanche, G. Peruzzo, G. Bader, and L. G. Caron, *J. Chem. Phys.* **77**, 3285 (1982).
- <sup>45</sup>H. Tanaka, T. Yamamoto, and T. Okada, *J. Phys. B* **14**, 2081 (1981).
- <sup>46</sup>J. W. Davenport, W. Ho, and J. R. Schrieffer, *Phys. Rev. Lett.* **17**, 3115 (1978).
- <sup>47</sup>E. Evans and D. L. Mills, *Phys. Rev. B* **5**, 4126 (1972); **7**, 853 (1973); Z. Lenac, M. Šunjić, D. Sokcovic, and R. Brako, *Surf. Sci.* **80**, 602 (1979).
- <sup>48</sup>H. Tanaka, S. K. Srivastava, and A. Chutjian, *J. Chem. Phys.* **69**, 5329 (1978).
- <sup>49</sup>K. Huang and A. Rhys, *Proc. R. Soc. London Ser. A* **204**, 406 (1950); J. J. Markham, *Rev. Mod. Phys.* **31**, 956 (1959).
- <sup>50</sup>P. H. Citrin, P. Eisenberger, and D. R. Hamann, *Phys. Rev. Lett.* **33**, 965 (1974).
- <sup>51</sup>W. R. Salaneck, C. B. Duke, W. Eberhart, E. W. Plummer, and H. J. Freund, *Phys. Rev. Lett.* **45**, 280 (1980), and references therein.
- <sup>52</sup>J. W. Gadzuk, *Phys. Rev. B* **14**, 5458 (1976).
- <sup>53</sup>J. W. Gadzuk, and M. Šunjić, *Phys. Rev. B* **12**, 524 (1975).
- <sup>54</sup>A. Chutjian, D. G. Truhlar, W. Williams, and S. Trajmar, *Phys. Rev. Lett.* **29**, 1580 (1972).
- <sup>55</sup>S. F. Wong and G. J. Schulz, *Phys. Rev. Lett.* **33**, 134 (1974).
- <sup>56</sup>R. S. Freund and W. Klemperer, *J. Chem. Phys.* **43**, 2422 (1965).
- <sup>57</sup>L. Sanche and G. J. Schulz, *Phys. Rev. Lett.* **26**, 943 (1971); *Phys. Rev. A* **6**, 69 (1972).
- <sup>58</sup>H. Ehrhardt, L. Laughans, F. Linder, and H. S. Taylor, *Phys. Rev.* **173**, 222 (1968).
- <sup>59</sup>H.-J. Law, J.-H. Foch, and E. E. Koch, *Chem. Phys. Lett.* **89**, 281 (1982).
- <sup>60</sup>D. Schmeisser and K. Jacobi, *Chem. Phys. Lett.* **62**, 51 (1979).
- <sup>61</sup>P. R. Norton, R. L. Tapping, H. P. Broida, J. W. Gadzuk, and B. J. Wacławski, *Chem. Phys. Lett.* **53**, 465 (1978).
- <sup>62</sup>W. R. Salaneck, *Phys. Rev. Lett.* **40**, 60 (1978).
- <sup>63</sup>C. B. Duke, *Surf. Sci.* **70**, 674 (1978).
- <sup>64</sup>D. F. Heller and S. Mukamel, *J. Chem. Phys.* **70**, 463 (1979); E. J. Heller and M. J. Davis, *J. Phys. Chem.* **84**, 1999 (1980).
- <sup>65</sup>A. Bianconi, M. Dell'Ariceia, P. J. Durham, and J. B. Pendry, *Phys. Rev. B* **26**, 6502 (1982).
- <sup>66</sup>For more information on electron scattering from isolated molecules, see H. S. W. Massey, *Electronic and Ionic Impact Phenomena* (Clarendon, Oxford, 1969), Vol. 2; L. G. Christophorou, *Atomic and Molecular Radiation Physics* (Wiley-Interscience, New York, 1971).